JOURNAL OF SOLID STATE CHEMISTRY 40, 143–151 (1981)

Reduction of the Titanium Niobium Oxides. II. $TiNb_{24}O_{62}$

S. K. E. FORGHANY* AND J. S. ANDERSON†

Inorganic Chemistry Laboratory, University of Oxford, Oxford, United Kingdom

Received April 13, 1981; in final form June 30, 1981

Interpretation of the reduction path of $TiNb_{24}O_{62}$ is complicated by uncertainty about both the stoichiometric ranges of the possible block structures and the formation of Ti–Nb solid solutions. Reduction forms the $Me_{12}O_{29}$ phase, probably from the outset, with an initial composition close to $Ti_2Nb_{10}O_{29}$, thereby rapidly depleting the $Me_{25}O_{62}$ phase of titanium. When $\log p_{O_2}$ (atm) has dropped to -9.62, a phase approximately $Ti_{0.95}Nb_{11.05}O_{29}$ is in equilibrium with titanium-free $Nb_{25}O_{62}$ at its lower composition limit ($NbO_{2.471}$). $Nb_{25}O_{62}$ is then reduced to $Nb_{47}O_{116}$ without change in the $Me_{12}O_{29}$. At $-9.62 > \log p_{O_2}$ (atm) > -10.0, niobium is transferred to the $Me_{12}O_{29}$ phase and $Nb_{47}O_{116}$ is consumed. A second univariant equilibrium is set up as $Nb_{47}O_{116}$ is reduced to $Nb_{22}O_{54}$. This is consumed in turn, to increase the niobium content of the $Me_{12}O_{29}$ until, at $\log p_{O_2}$ close to -10.8, monophasic $Ti_{0.48}Nb_{11.52}O_{29}$ is formed. The $(Ti,Nb)O_2$ solid solution then appears and the final product is $Ti_{0.04}Nb_{0.96}O_2$, with the rutile superstructure cell reported for NbO_2.

In an earlier paper (*1*) we have discussed the changes of structure that are imposed when $TiNb_2O_7$ and $Ti_2Nb_{10}O_{29}$ undergo reduction, and also the form of that portion of the TiO_2–NbO_2–$NbO_{2.5}$ equilibrium diagram, with $2.417 \geq x$ (in MeO_x) > 2. For $x > 2.417$, not only is the equilibrium diagram more complex, but the phases that enter into it are not fully characterized. As a consequence, the route traversed during the reduction of $TiNb_{24}O_{62}$ ($x = 2.480$) is less readily interpreted. There is a multiplicity of block structures and regular intergrowth phases in this stoichiometric range and, in addition, it is uncertain how far randomly intergrown Wadsley defects can contribute, under equilibrium conditions, to stoichiometric variability. There is little detailed knowledge about the ability of the $NbO_{2.5}$–NbO_2 and the $NbO_{2.5}$–TiO_2 limiting binary systems to form extensive ranges of solid solutions. As is shown below, the $Me_{12}O_{29}$ structure (Me = Nb + Ti) is formed as one clearly defined, monophasic stage in the reduction of $TiNb_{24}O_{62}$; the route traversed in reaching this stage would not have been predicted.

Kimura's thermodynamic measurements at 1400°C (*2*) define the equilibria between, and the stoichiometry of, the phases in the limiting $NbO_{2.5}$–NbO_2 binary system. These are summarized in Table I. These results confirmed Gruehn's finding (*3*) that, notwithstanding the apparently uniquely defined composition of the block structures, H-Nb_2O_5 (and also $Nb_{22}O_{54}$) has a significant existence range, on the niobium-excess side, and that the ideal composition

* Present address: Tussenafdeling der Metaalkunde, Technische Hogeschool, Rotterdamseweg 137, Delft, The Netherlands.

† Present address: Research School of Chemistry, Australian National University, P.O. Box 4, Canberra, A.C.T. 2600 Australia.

0022-4596/81/140143-09$02.00/0

TABLE I

STOICHIOMETRIC RANGES AND STABILITY RANGES OF BINARY NIOBIUM OXIDES

Phase	Block structure type	Composition range	log p_{O_2} (atm)
$Nb_{28}O_{70}$ (H-Nb_2O_5)	$(5 \times 3)_\infty + (4 \times 3)_1$	$NbO_{2.500}$–$NbO_{2.490}$	> -8.11
$Nb_{53}O_{132}$	$\{(5 \times 3)_\infty + (4 \times 3)_1\} + (4 \times 3)_2$	$NbO_{2.484}$–$NbO_{2.483}$	-8.11– -8.52
$Nb_{25}O_{62}$	$(4 \times 3)_2$	$NbO_{2.476}$–$NbO_{2.470}$	-8.52– -9.62
$Nb_{47}O_{116}$	$(4 \times 3)_2 + \{(4 \times 3)_\infty + (3 \times 3)_1\}$	$NbO_{2.468}$	-9.62– -9.98
$Nb_{22}O_{54}$	$(4 \times 3)_\infty + (3 \times 3)_1$	$NbO_{2.453}$–$NbO_{2.446}$	-9.98–-10.81
$Nb_{12}O_{29}$	$(4 \times 3)_\infty$	$NbO_{2.417}$	-10.81–-10.94
NbO_2	—	$NbO_{2.0}$	< -10.94
$Nb_{39}O_{97}$	$\{(5 \times 3)_\infty + (4 \times 3)_1\} + 2(4 \times 3)_2$	(Ideal $NbO_{2.487}$) Actual?	Uncertain thermodynamic status
$Nb_{84}O_{207}$	$2(4 \times 3)_3 + (3 \times 3)_1$	(Ideal $NbO_{2.464}$)	Metastable, transitional intergrowths
$Nb_{59}O_{145}$	$(4 \times 3)_4 + (3 \times 3)_1$	(Ideal $NbO_{2.458}$)	

falls outside the stable existence range of $Nb_{53}O_{132}$, $Nb_{25}O_{62}$, $Nb_{47}O_{116}$ (and probably $Nb_{39}O_{97}$); Gruehn considered that the $Nb_{25}O_{62}$ moiety in the intergrowth structures is inherently substoichiometric. Although Kimura discussed the observed stoichiometric variability in terms of point defect equilibria, the crystal structure of the inherently substoichiometric phase "$GeO_2 \cdot 9Nb_2O_5$" (*4*) suggests a common principle underlying all metal-excess block structures: if octahedral sites in the corners of the channels between blocks can be occupied, instead of the central row of tetrahedral sites, extra cations can be accommodated. The evidence indicates that a limit to this "stuffing" of the channels is reached with about 10% extra cations.

In the other limiting binary system, Nb_2O_5–TiO_2, the phases $TiNb_{52}O_{132}$ and $TiNb_{24}O_{62}$ are known, but no compound has been found intermediate between $TiNb_{24}O_{62}$ and $Ti_2Nb_{10}O_{29}$. There is no published evidence as to whether $TiNb_{24}O_{62}$ is strictly stoichiometric or whether, like $Nb_{25}O_{62}$, it has a composition range and, if so, whether that range extends to the ideal composition. Gruehn (*3*) has referred to solid solutions in the $Me_{25}O_{62}$ and $Me_{53}O_{132}$ structure types, and it is to be expected that these should span the full range of substitution of Ti(iv) for Nb(iv). It is not known whether Ti(iv) can be substituted for Nb(iv) in the $Nb_{22}O_{54}$ and $Nb_{47}O_{116}$ structures.

These uncertainties about the stable existence range of $TiNb_{24}O_{62}$ and its solid solutions are relevant in the present work. The $TiNb_{24}O_{62}$ used was prepared to the exact stoichiometry $TiO_2 + 12Nb_2O_5$; it was monophasic in its X-ray diffraction pattern and high-resolution electron microscopy afforded no evidence that it had a significant concentration of Wadsley defects of *H*-Nb_2O_5 (or $Me_{53}O_{132}$) structure. Gruehn's interpretation of the Nb_2O_5–$Nb_{12}O_{29}$ binary would imply that, in material of total composition $MeO_{2.480}$, regions of real composition $NbO_{2.476}$ should be balanced by intergrowths of $Nb_{28}O_{70}$. The homogeneity of our material implies that the titanium-rich end of the solid solutions is stable at the ideal composition $MeO_{2.480}$; if so the oxy-

gen-rich limit of its solid solutions with $NbO_{2.476}$ necessarily varies across the equilibrium diagram. About the oxygen-poor limit of the solid solutions, there is no evidence, and how the initial stages of reduction are interpreted unavoidably depends upon the assumptions made about the stoichiometric variability of $TiNb_{24}O_{62}$.

Experimental

In general, all experimental procedures followed those described in Ref. (*1*).

A 20-g sample of $TiNb_{24}O_{62}$ was prepared from Specpure TiO_2 and Nb_2O_5, in the exact molar ratio 1 : 12, by repeated firing at 1400°C, grinding and remixing. Four hundred-milligram samples were equilibrated at 1400°C with metered CO/CO_2 buffers, using a constant flow rate, and were rapidly quenched. The buffers covered the range of oxygen fugacities $-6.0 \geq \log p_{O_2}$ (atm) ≥ -11.0. After each reduction, the products were analyzed for their total oxygen/metal ratio, by reoxidation on a Cahn RG4 thermobalance.

For purposes of phase analysis, X-ray diffraction patterns were recorded at a number of points along the reduction path, using a Hägg–Guinier camera with monochromatized Cu$K\alpha$ radiation.

A number of the reduction products was also examined by high-resolution structure imaging electron microscopy. The samples were finely crushed and dispersed on to reticular carbon films. Images at about 0.35-nm resolution were taken with a JEM 100B electron microscope, following the techniques that are now standard practice. Structure imaging microscopy, and selected area electron diffraction from individual crystals, did not provide a phase analysis, but they supplemented the X-ray diffraction methods by sampling the structure, thereby detecting the possible intergrowth of different structure elements that can coexist in thermodynamic equilibrium.

Results

Figure 1 shows how the composition of the reduction product MeO_x varies with the equilibrium oxygen fugacity. As in the previous work on the reduction of $TiNb_2O_7$ and $Ti_2Nb_{10}O_{29}$, it would be possible to join the experimental points by a smooth curve which, in this case, has four distinct segments and simulates two consecutive bivariant processes.

X-Ray diffraction showed block structures to be present throughout the reduction process. Along the initial segment A–B–C, the patterns were those of the $Me_{25}O_{62}$ structure, but weak lines due to some other phase(s) were visible for materials MeO_x, $x < 2.47$. In two samples, marked y in Fig. 1, diffraction lines of the $Me_{12}O_{29}$ phase were definitely identified. Selected area electron diffraction patterns from single crystal flakes confirmed the presence of $Me_{25}O_{62}$ as the predominant phase, down to a composition $MeO_{2.45}$, but at the composition marked x in Fig. 1, crystals were found that showed the diffraction pattern of $Me_{53}O_{132}$. At some stage between C and Q, the $Me_{12}O_{29}$ X-ray diffraction pattern became dominant, and no other block structure than $Me_{12}O_{29}$ could be detected with certainty along the segment Q–E–F. At F, the reduction product is monophasic $Ti_{0.48}Nb_{11.52}O_{29}$ and thereafter the reduction of the $Me_{12}O_{29}$ solid solution, eventually to the dioxide phase

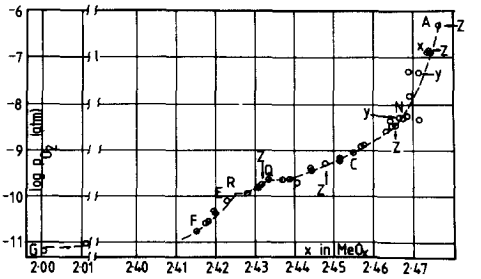

FIG. 1. Oxygen/metal ratio in reduced $TiNb_{24}O_{62}$ as function of the equilibrium oxygen pressure.

$Ti_{0.04}Nb_{0.96}O_2$. The X-ray diffraction pattern of this product could be indexed in terms of the large rutile superstructure cell assigned by Marinder (*5*) to NbO_2.

If these results are to be fitted into an equilibrium diagram, some assumption must be made about the stoichiometry of the $TiNb_{24}O_{62}$–$Nb_{25}O_{62}$ solid solutions. The first alternative (Fig. 2A) is that $TiNb_{24}O_{62}$ extends to the ideal composition and, like $Nb_{25}O_{62}$, has an accessible range of composition through the "stuffing" of extra cations in the channels of tetrahedral sites. In this case, the very first stages of reduction would not involve the elimination of some second phase, richer in TiO_2 (in this case, $Ti_2Nb_{10}O_{29}$), but would abstract oxygen directly; cations would be injected into octahedral channel sites as part of the structure was dismantled. Thus only one solid phase would be present and the system would be *trivariant*. The implication of the extra degree of freedom would be that the composition was no longer completely specified by the experimental conditions; any local composition corresponding to any point on the oxygen isobar for the gas buffer used would be in equilibrium, provided that the total composition of the crystal remained constant. In other words, fluctuations would be permitted, local disproportionation into TiO_2-richer and TiO_2-poorer regions. Only when the total composition reached the point N would a new phase ($Me_{12}O_{29}$) appear, and the system would follow normal, bivariant behavior.

The alternative extreme hypothesis is that the $TiNb_{24}O_{62}$ structure has the ideal composition, with no stoichiometric range: that variability of composition, through channel stuffing, can arise only as Nb(iv) is introduced in solid solution. The phase field would then have the form shown schematically in Fig. 2B. On that model, an $Me_{12}O_{29}$ phase, probably $Ti_2Nb_{10}O_{29}$ in the first place, would be eliminated from the beginning of reduction, but calculation shows that the amount of this second phase would be too small to detect by X-ray diffraction, throughout the segment A–B of Fig. 1. There is little evidence to discriminate between the alternative models; electron microscope findings are discussed below.

Because the second solid phase is richer in titanium than $TiNb_{24}O_{62}$, the ratio Nb/Ti in the $Me_{25}O_{62}$ phase is progressively raised; the composition shifts to the right along the solvus line (Fig. 3), while the coexisting $Me_{12}O_{29}$ phase also becomes enriched in niobium. At N (log p_{O_2} = −8.25

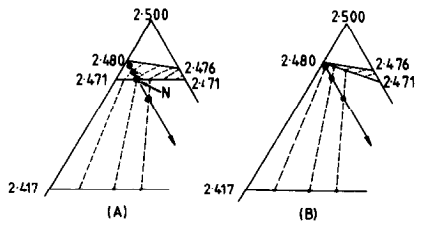

FIG. 2. Alternative hypotheses for the initial stages of reduction of $TiNb_{24}O_{62}$. (A) In the $NbO_{2.5}$–TiO_2 binary, the $TiNb_{24}O_{62}$ phase has a broad phase range, analogous to that of $Nb_{25}O_{62}$. (B) $TiNb_{24}O_{62}$ has a negligible composition range, which broadens as the niobium content increases in the solid solutions.

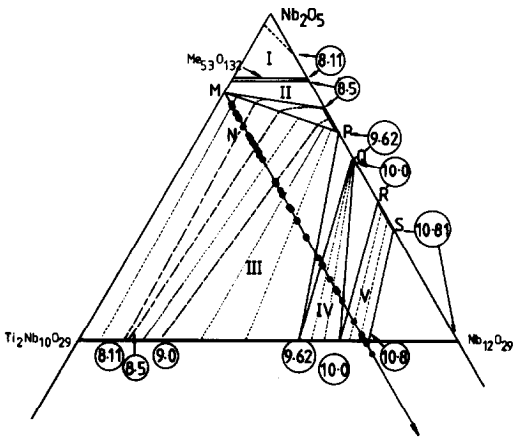

FIG. 3. Proposed equilibrium diagram for the $NbO_{2.5}$–NbO_2–TiO_2 system, oxygen/metal ≥2.417. Reduction trajectory of $TiNb_{24}O_{62}$ shown with experimental points. Composition and structure of the block structure change along route M–P–Q–R–S–$Ti_{0.48}Nb_{11.52}O_{29}$.

atm), its composition is around $Ti_{1.8}Nb_{10.2}O_{29}$. By the stage where the oxygen fugacity has dropped to log p_{O_2} = −9.62, the $Me_{25}O_{62}$ composition has reached the point P, on the limiting $NbO_{2.5}$–NbO_2 binary line; $Ti_{0.95}Nb_{11.05}O_{29}$ is in equilibrium with $Nb_{25}O_{62}$ (at its lower limiting composition), free from titanium, which has been trasferred completely into the $Me_{12}O_{29}$ phase.

From this point onward, the phase equilibria are determined by the thermodynamics of the Nb_2O_5–NbO_2 binary system. The next step, along P–Q, is the univariant reduction of $Nb_{25}O_{62}$ to $Nb_{47}O_{116}$, leaving the $Me_{12}O_{29}$ phase unaltered in composition or quantity. A step on the reduction curve (Fig. 1, P–Q) corresponds to that process. The next stage of reduction transfers niobium (iv) from the $Nb_{47}O_{116}$ to the $Me_{12}O_{29}$ phase, which changes in composition to around $Ti_{0.6}Nb_{11.4}O_{29}$ as the oxygen fugacity drops across the very narrow phase range of $Nb_{47}O_{116}$. At log p_{O_2} = −10.0, a second univariant phase field Q–R is entered; the only reaction is the reduction of $Nb_{47}O_{116}$ to $Nb_{22}O_{54}$. This should take place at R in Fig. 1, but the univariant step involves only a small change in the total composition, and is masked by the spacing between experimental points. Across the relatively broad phase range of $Nb_{22}O_{54}$, R–S, continued reduction transfers niobium to the $Me_{12}O_{29}$ phase until, at S (log p_{O_2} slightly higher than −10.8), all the $Nb_{22}O_{54}$ phase has been consumed and the reduction product converted into monophasic $Ti_{0.48}Nb_{11.52}O_{29}$. The oxygen fugacity at this point is very close to that at the lower existence limit of $Nb_{22}O_{54}$, implying that it is almost independent of composition across the niobium-rich end of the $Me_{12}O_{29}$ solid solution.

Table II summarizes the approximate phase compositions, and the amount of oxygen removed by reduction, per unit of $TiNb_{24}O_{62}$, at various stages in this sequence of processes. This table, and Fig. 3, are based upon a strictly classical interpretation of phase equilibria; how far they need modification, to allow for the versatile capacity of block structures for coherent intergrowth, can be checked only by observation of the real-space microstructure of the materials.

Evidence from X-ray and electron diffraction, and from electron microscopy, does not unequivocally settle the composition limits of the $Me_{25}O_{62}$ solid solutions. If the two end members, "$Nb_{25}O_{62}$" and "$TiNb_{24}O_{62}$" were strictly analogous, our original sample composition TiO_2 + $12Nb_2O_5$ should be a biphasic mixture of about 64 mole% $(Ti,Nb)O_{2.476}$ + 36 mole% $(Ti,Nb)O_{2.487}$; whereas its X-ray diffraction pattern was that of the monophasic $Me_{25}O_{62}$ structure. On that evidence, we consider that the $TiNb_{24}O_{62}$ phase at least extends to the ideal composition.

Reduction products were examined by

TABLE II

Point	log p_{O_2}	Phases present	No. of 0 atoms removed per unit of $TiNb_{24}O_{62}$
M	—	$TiNb_{24}O_{62}$	0
N	−8.24	$0.2(Ti_{1.8}Nb_{10.2}O_{29})$ + $0.90(Ti_{0.71}Nb_{24.29}O_{61.8})$	0.36
P	−9.62	$1.25(Ti_{0.8}Nb_{11.2}O_{29})$ + $0.40(Nb_{25}O_{61.75})$	1.05
Q	−9.62	$1.25(Ti_{0.8}Nb_{11.2}O_{29})$ + $0.21(Nb_{47}O_{115.8})$	1.09
	−10.0	$1.70(Ti_{0.6}Nb_{11.4}O_{29})$ + $0.099(Nb_{47}O_{115.8})$	1.36
R	−10.0	$1.70(Ti_{0.6}Nb_{11.4}O_{29})$ + $0.21(Nb_{22}O_{53.97})$	1.40
S	−10.8	$2.083(Ti_{0.48}Nb_{11.52}O_{29})$	1.58

electron microscopy at a few stages in the process, marked Z in Fig. 1. If $TiNb_{24}O_{62}$ has any existence range on the metal excess side, the most lightly reduced sample, $MeO_{2.474}$ (log $p_{O_2} = -6.81$) should be either monophasic or have $Me_{12}O_{29}$ as a second phase. Of nine crystals examined, eight gave the electron diffraction pattern of $Me_{25}O_{62}$, without streaks or evidence for defect structure; structure images showed the $(4 \times 3)_2$ block structure, without any Wadsley defects. One crystal was found, however, which had the diffraction pattern, and furnished a structure image, of $Me_{53}O_{132}$. At the total composition $MeO_{2.464}$ (log $p_{O_2} = -8.42$), the reduction products should, on any hypothesis, be a biphasic mixture of the $Me_{25}O_{62}$ phase with small amounts of the $Me_{12}O_{29}$. One of seven crystals examined, however, gave the structure image shown in Fig. 4. Not only are structure elements of the $Nb_{28}O_{70}$ structure intergrown with $Me_{25}O_{62}$, but they are locally ordered in such a way as to display a composition gradient across the region imaged. The strip X has the $Me_{53}O_{132}$ structure, strip Y the $Me_{39}O_{97}$ structure, and in Z isolated files of $Nb_{28}O_{70}$ form Wadsley defects in $Me_{25}O_{62}$. If we accept Gruehn's values for the limiting compositions of these structures (Ref. (*3*) and Table I), the average composition of the region imaged would be approximately $MeO_{2.477}$; this lies close to the upper boundary of the $Me_{25}O_{62}$ phase, as sketched in Fig. 3, suggesting that the range of oxygen/metal ratios, in the

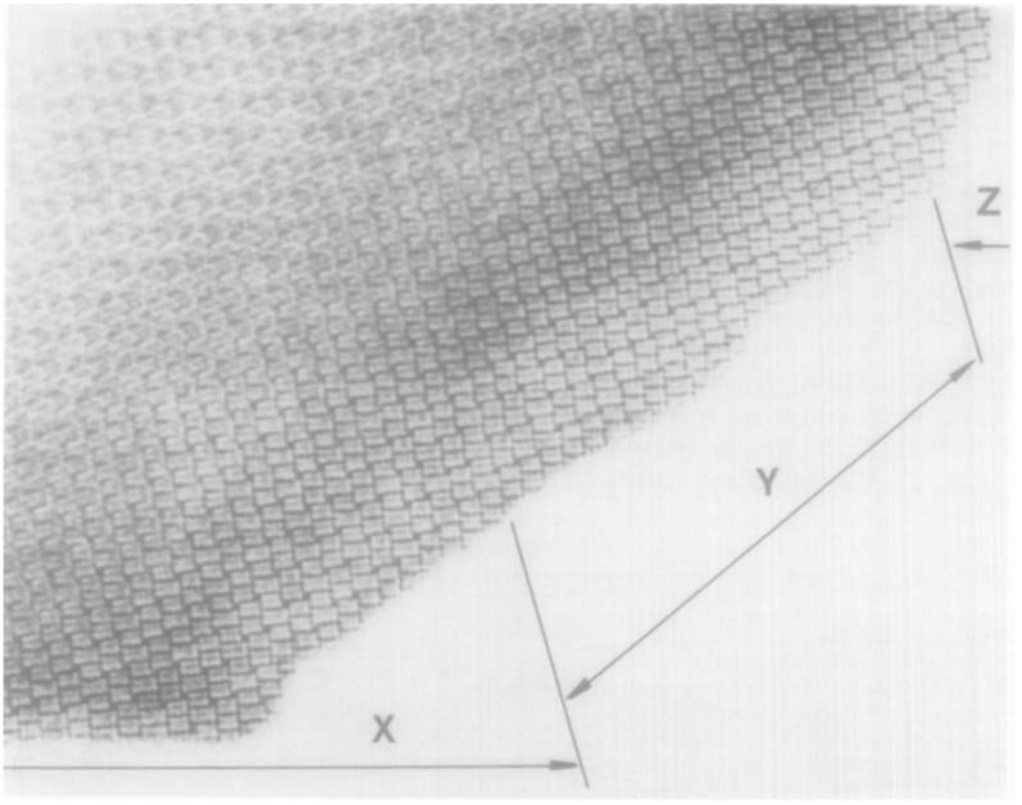

FIG. 4. Electron micrograph from reduction product $MeO_{2.464}$. X is a domain of $Me_{53}O_{132}$; Y is a domain of $Me_{39}O_{97}$; to the right of Z, $Me_{25}O_{62}$ structure with occasional Wadsley defects of $Me_{53}O_{132}$.

titanium-rich solid solutions, may be narrow. Unexplained, however, is the structural inhomogeneity of the material after long heat treatment (15 hr at 1400°C), as compared with the efficiency with which the binary niobium oxides undergo phase separation at the same temperature (compare Ref. (*2*)).

Micrographs at the residue compositions $MeO_{2.448}$ and $MeO_{2.431}$ give some evidence about later stages in the reduction reaction. From Fig. 3, $MeO_{2.448}$ should be biphasic ($Me_{12}O_{29}$ + $Me_{25}O_{62}$ almost denuded of titanium) and close to the point at which $Nb_{47}O_{116}$ should begin to be formed. Figure 5 is a micrograph from one crystal of this material. It shows domains or slabs of monoclinic $Nb_{12}O_{29}$, rather regular in breadth, coherently intergrown with narrow strips of a new kind of nearly regular structure. This contains $(3 \times 3)_1$ blocks, dispersed among (4×3) blocks which are linked in short strings; these are structure elements that would be needed to build up the $Nb_{47}O_{116}$ structure, and the new structure can be regarded as either a precursor or a relic of $Nb_{47}O_{116}$. Two new and related superstructures are thereby formed, in small domains. That marked Y has the unit cell composition $Me_{84}O_{207}$ ($MeO_{2.464}$); Z is $Me_{59}O_{145}$ ($MeO_{2.458}$); compare $Nb_{47}O_{116}$ $MeO_{2.463}$. From a count of block sizes, the gross composition of the region shown is about $MeO_{2.45}$, which is close to the analyzed composition of the whole sample. This suggests that the coherent intergrowth of stable reaction products with metastable precursor structures is a viable structural alternative to the separation of discrete, stable phases, as would be postulated by classical thermodynamics. This sample had been annealed for 17 hr at 1400°C, but the fluctuations of structure (and of local, though not of gross composition) had not disappeared, nor had coherence been lost between the growing product structure and the structure being dismantled.

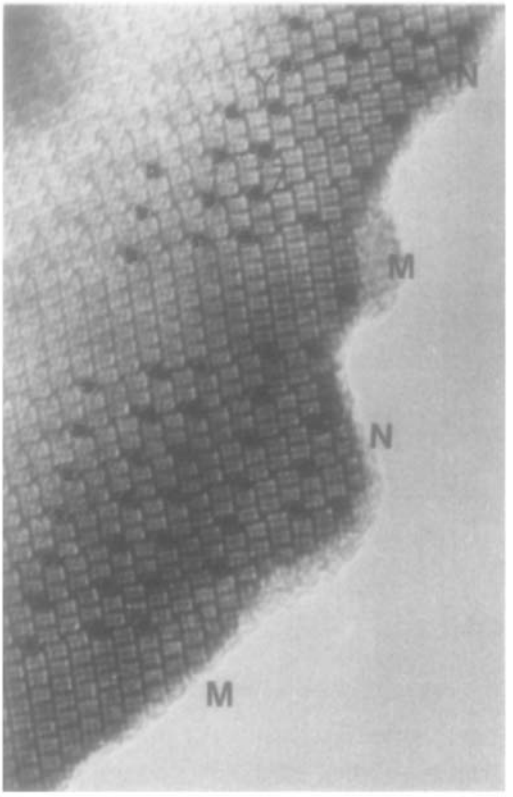

FIG. 5. Electron micrograph from reduction product $MeO_{2.448}$. M, M domains of $Me_{12}O_{29}$ structure, coherently intergrown with domains N, N containing elements of the $Me_{22}O_{54}$ structure, ordered into a superlattice.

The reduction reaction is itself a homogeneous solid-state process. It must be inferred that the transformation of a coherently intergrown domain structure into an assembly of discrete phases, in the sense used by Willard Gibbs, may be associated with only a small change in the free energy of the system.

The material $MeO_{2.431}$ is close to Q in Fig. 1, and should contain $Me_{12}O_{29}$ and $Me_{22}O_{54}$ as discrete phases. Fig. 6 is a micrograph from a crystal, nominally of monoclinic (and extensively twinned) $Nb_{12}O_{29}$, showing a small domain of (3×3) blocks, which is essentially an intergrowth of $Nb_{22}O_{54}$. This is the complementary, and disappear-

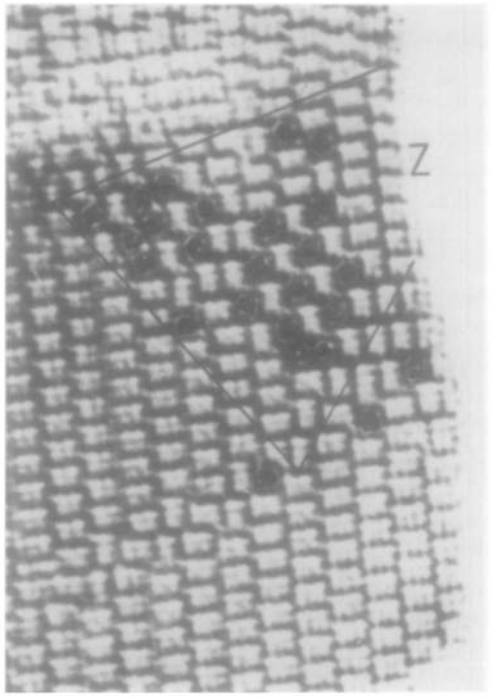

FIG. 6. Electron micrograph from reduction product $MeO_{2.431}$. A coherently intergrown domain of $Me_{22}O_{54}$ structure Z in twinned $Me_{12}O_{29}$ structure.

ing, phase, and the domain shown is a relic, trapped by completion of the homogeneous processes around it.

These observations have a wider bearing on the operational aspect of phase equilibrium studies on systems which can exhibit coherent intergrowth, between the members of a family of related, chemically interconvertible structures. In such systems, the course of the reaction and the final state (not necessarily true equilibrium) may be determined by mechanistic factors.

Classical thermodynamics treats of the equilibrium attained when a structurally ideal reactant A is converted into a structurally ideal product B. If the structures of A and B are such that they can intergrow coherently, the heterogeneous processes that form structure B as a discrete phase may be mechanistically and kinetically less favorable than some homogeneous processes. Two possibilities then arise. (a) The structure A is changed directly into structure B by purely local displacements of atoms, without disrupting the continuity of the crystal structure; coupled with this must be some transport process, whereby the crystal is depleted (or enriched) in some species of atoms, to change its composition. Domains of B are then formed as coherent intergrowths in structure A. These grow until the roles of matrix and intergrowth are reversed, and relict domains of A become intergrown in B as each crystalline particle approaches complete conversion. This is the situation to be seen in Fig. 6. (b) Either because there is a strong tendency (i.e., an energetic gain) for local ordering, or because the reaction mechanism itself exercises a strong topochemical control, the product structure B is formed by way of one or more metastable precursor structures, intergrown as domains that show some kind of superlattice. In Fig. 5, the superlattices are two members of a hypothetical homologous series $a\{(4 \times 3)_m\} + (3 \times 3)_1$, corresponding to the values $a = 2, m = 3$ for $Me_{84}O_{207}$ and $a = 1, m = 4$ for $Me_{59}O_{145}$, in which (3×3), blocks are intergrown with progressively longer ribbons of (4×3) blocks, as the composition moves towards the limit $MeO_{2.417}$. The same structure elements are seen in $Me_{47}O_{116}$ $(a = 1\, m = 3)$ and in $Nb_{22}O_{54}$ $(a = 1, m = \infty)$.

The micrograph shows domains of the simplest intermediate ordering patterns, in which elements of the original $Me_{25}O_{62}$ block configuration persist, intergrown with domains of the ultimate product structure.

Thermodynamically, such a protean structure would behave as a pseudo-bivariant system, and an equilibrium diagram, such as Fig. 3, based on classical treatment of equilibria is an idealization. Since the structures concerned were found after high-temperature annealing, it would appear that

the factors distinguishing the domain structures from classical biphasic systems—interfacial energies between domains, fluctuations of composition and structure, degree of ordering etc.—do not profoundly affect the thermodynamic equilibria.

Acknowledgments

S.K.E.F. would thank the Iranian Ministry of Science and Higher Education, and also the British Council, for their support.

References

1. S. K. E. Forghany and J. S. Anderson, *J. Solid State Chem.* **40**, 136 (1981).
2. S. Kimura, *J. Solid State Chem.* **6**, 438 (1973).
3. R. Gruehn, N.B.S. Special Publ. **364**, Solid State Chemistry (1972).
4. J. S. Anderson, D. J. M. Bevan, A. K. Cheetham, R. B. Von Dreele, J. L. Hutchison, and J. Strähle, *Proc. Roy. Soc. A* **346**, 139 (1975).